

# Nonlinear transport imaging by scanning impedance microscopy

J. Shin<sup>a)</sup>

Condensed Matter Sciences Division, Oak Ridge National Laboratory, Oak Ridge, Tennessee 37831 and  
Department of Physics and Astronomy, The University of Tennessee, Knoxville, Tennessee 37996

V. Meunier

Computer Science and Mathematics Division, Oak Ridge National Laboratory,  
Oak Ridge, Tennessee 37831

A. P. Baddorf and S. V. Kalinin

Condensed Matter Sciences Division, Oak Ridge National Laboratory, Oak Ridge, Tennessee 37831

(Received 17 June 2004; accepted 1 September 2004)

Scanning probe microscopy is an established tool for characterization of the *linear* static and frequency-dependent lateral electronic transport in materials and devices at the nanoscale. In this letter, a modified scanning impedance microscopy (SIM) technique is proposed to extend the nanoscale transport measurements of intrinsic material properties to the *nonlinear* regime, through detection of frequency harmonics, and exemplified by a detailed study of a prototypical metal–semiconductor interface. The imaging mechanism, surface–tip contrast transfer, optimal experimental conditions, and potential applications of nonlinear SIM are discussed. This technique can be readily transferred to most cantilever-based scanning probe microscopes. © 2004 American Institute of Physics. [DOI: 10.1063/1.1812372]

Electronic transport in materials and devices is often governed by a limited number of electrically active interfaces, such as metal–semiconductor contacts in electronic devices,<sup>1</sup> grain boundaries,<sup>2–4</sup> or atomic defects in carbon nanotubes and other one-dimensional structures.<sup>5</sup> In the last decade, scanning probe microscopy (SPM) techniques such as scanning surface potential microscopy were demonstrated to be powerful tools for quantitative dc transport imaging in semiconductor structures<sup>6,7</sup> and at grain boundaries.<sup>8,9</sup> An approach for frequency-dependent transport imaging, referred to as scanning impedance microscopy (SIM), was also developed.<sup>7,10</sup> Notably, SPM techniques have been exclusively used to access the linear dc or ac transport properties, while current–voltage transport properties of most electroactive interfaces are intrinsically nonlinear, a highly desired property for device functionality. Here, we propose an extended SIM approach for the quantitative real space imaging of frequency-dependent nonlinear transport behavior at electroactive interfaces.

Nonlinear SIM is implemented on a commercial SPM system (Veeco MultiMode NS-III A) equipped with a function generator and a lock-in amplifier (DS 345 and SRS 830, Stanford Research Instruments). As a test for the technique, we used a prototypical metal–semiconductor interface prepared by cross-sectioning a commercial Au–Si Schottky diode and connected in series with two current limiting resistors,  $R=1, 3, 10,$  or  $30$  k $\Omega$ , as illustrated in Fig. 1(a). Measurements were performed using Pt coated tips (NCSC-12 F, Micromasch,  $l \approx 250$   $\mu\text{m}$ , resonant frequency  $\sim 41$  kHz) in the dual-pass mode with typical lift height of 200 nm. A lock-in amplifier is used to determine the magnitude and phase of the cantilever response at the first, second, and third harmonic of the modulation signal applied across the circuit. The output amplitude,  $A_{n\omega}$ , and phase shift,  $\theta_{n\omega}$ , where  $n$  is the order of the harmonic, are recorded by the

AFM electronics. To ensure strong mechanical response of the cantilever for weak higher-harmonic signals while avoiding cross-talk between electrostatic and topographic data, the frequency of the ac modulation voltage was selected such that the mechanical response of the cantilever occurs at the first resonance frequency ( $\omega_{r1}=39$  kHz), whereas topographic imaging is performed at the second resonance frequency ( $\omega_{r2}=270$  kHz) of the cantilever. Given that the eigenfrequencies for the cantilever are not an integral of the primary resonance frequency, this approach decouples electrostatic and mechanical signals while taking advantage of the resonance amplification for both of them. Practically, high harmonic signals can be measured for modulation volt-

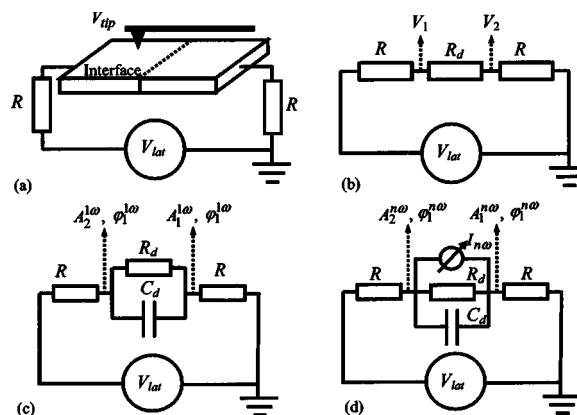


FIG. 1. (a) Experimental setup for dc and ac SPM transport measurements. (b) Equivalent circuit for SSPM based dc transport measurements. The tip measures the dc potential distribution induced by a lateral bias applied across the sample, thus imaging resistive elements of the equivalent circuit. (c) Equivalent circuit for linear SIM measurements. The tip measures the distribution of the phase and amplitude of the ac voltage, thus imaging the resistive and capacitive elements of equivalent circuit. (d) Equivalent circuit for nonlinear SIM. The tip measures the higher harmonics of potential oscillations in the sample generated due to frequency mixing on nonlinear interfaces, which act as current sources at harmonics of the applied bias.

<sup>a)</sup>Electronic mail: jshin4@utk.edu

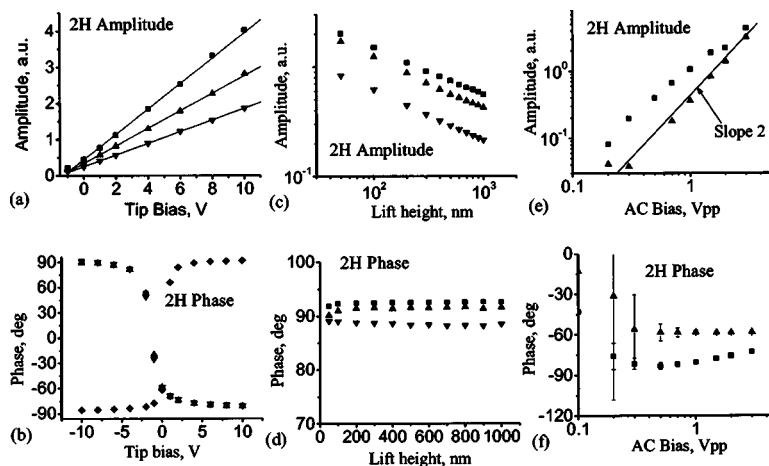


FIG. 2. The tip bias dependence of (a) amplitude and (b) phase of second-harmonic cantilever oscillations for lift height 100 nm (■), 200 nm (▲), and 500 nm (▼) on the biased part of the interface and (◆) on the grounded part of the interface. Note a 180° phase shift across the interface. Lift height dependence of amplitude (c) and phase (d) of the second harmonic of tip oscillations for tip biases of 10 V (■), -10 V (▲), 3 V (▼). The ac bias dependencies of (e) amplitude and (f) phase of the response for  $V_{dc}=0$  (■) and  $V_{dc}=-4$  V (▲).

ages as small as 50 mV<sub>pp</sub> (i.e., in the true small signal limit).

In nonlinear SIM, a lateral modulation bias  $V_{lat}=V_{dc}+V_{ac}\cos(\omega t)$  is applied across the circuit shown in Fig. 1. Application of a lateral bias establishes dc,  $V_{0\omega}(x)$  and ac,  $V_{1\omega}(x)$ , potential distributions across the system, where  $x$  is a spatial coordinate. The dc potential distribution is determined solely by the resistive elements of the equivalent circuit [Fig. 1(b)], whereas  $V_{1\omega}$  is determined by resistive and capacitive elements [Fig. 1(c)]. Thus, simultaneous mapping of the two can be used to, e.g., locally determine the  $C-V$  characteristic of the interface.<sup>7</sup> At the same time, the intrinsically nonlinear nature of the interface will result in the appearance of higher-order harmonics of the applied potential at  $2\omega, 3\omega, \dots$ . Specifically, the surface potential of the system can be written as

$$V_{surf} = V_{0\omega} + \sum_{n=1} V_{n\omega} \cos(n\omega t + \varphi_{n\omega}), \quad (1)$$

where  $V_{n\omega}$  is the amplitude and  $\varphi_{n\omega}$  the phase of the  $n$ th harmonic of surface potential. The oscillating bias results in capacitive force acting on the dc biased tip,

$$2F_{cap}(z) = C'_z(V_{tip} - V_{surf})^2. \quad (2)$$

The nonlinear SIM apparatus measures the phase and amplitude of the tip oscillations of the different harmonics, as found by combining Eqs. (1) and (2). For  $\varphi_{n\omega}=0$ ,

$$F_{1\omega} \sim 2(V_{tip} - V_{0\omega})V_{1\omega} + V_{1\omega}V_{2\omega} + V_{2\omega}V_{3\omega} + \dots, \quad (3a)$$

$$F_{1\omega} \sim 2V_{2\omega}(V_{tip} - V_{0\omega})0.5V_{1\omega}^2 + V_{1\omega}V_{3\omega} + \dots, \quad (3b)$$

$$F_{3\omega} \sim 2V_{3\omega}(V_{tip} - V_{0\omega}) + V_{1\omega}V_{2\omega} + \dots. \quad (3c)$$

The higher harmonics of the force arise from the convolution of the nonlinear behaviors of the electroactive interface and of the tip-surface junction. In general, the magnitude of high order harmonics decreases with order,  $V_{1\omega} \gg V_{2\omega} \gg V_{3\omega}$ ; hence only the first term in Eq. (3a) is significant while the first and second terms dominate in Eqs. (3b) and (3c). The second and third order harmonic signals can be represented by the sum of an intrinsic frequency mixing signal generated in the device,  $F_{n\omega}^{int}$ , and a signal generated in the tip-surface junction,  $F_{n\omega}^j$ , as  $F_{n\omega} = F_{n\omega}^{int} + F_{n\omega}^j = 2V_{n\omega}(V_{tip} - V_{0\omega}) + V_{1\omega}V_{(n-1)\omega}$ . Hence, the tip-bias dependence of the

cantilever oscillation amplitude leads to an explicit separation of the intrinsic and junction contributions. A third harmonic signal can only be observed for intrinsically nonlinear interfaces and therefore constitutes an unambiguous signature of nonlinearity in the material.

Similar linear SIM, the amplitude of the tip vibrations is proportional to the corresponding harmonic of the bias, while the phase is shifted by a position-independent term. Thus, measuring the phase and amplitude of the tip oscillation allows the phase and amplitude of surface voltage oscillations to be mapped. By choice, the mechanical resonance in the amplitude for the  $n$ th harmonic signal occurs at the driving frequency,  $\omega = \omega_0/n$ , and the experimental conditions can be tuned for selective measurement of the chosen harmonics. Alternatively, for large driving signal higher-order harmonics can be measured as a function of frequency, providing information on frequency-dependent nonlinear transport at the interfaces.

The applicability of nonlinear SIM is illustrated in Fig. 2(a). As predicted by Eq. (3b), the response amplitude for the second harmonic is a linear function of the tip bias, the slope of which is proportional to the tip-surface separation. The phase of the tip oscillations [Fig. 2(b)] changes by 180° between positive and negative biases and does not depend on the tip-surface separation. The second harmonic amplitude decreases with the tip surface separation,  $z$ , as  $\sim z^{-0.5}$ , which is consistent with a spherical model for the tip, while the phase of the tip oscillations is virtually distance independent [Figs. 2(c) and 2(d)]. Finally, shown in Figs. 2(e) and 2(f) are the ac bias dependencies of the amplitude and phase of the response. Generally, a dimensional argument indicates that  $A_{n\omega}$  is proportional to  $V_{ac}^n$ . Experimentally, the corresponding power strongly depends on the lateral dc bias across the interface.

In order to get further insight into the fundamental mechanism of nonlinear SIM, we consider the harmonic generation at an electroactive interface. For small probing biases, the  $I-V$  curve of the interface can be expanded in a Taylor series as  $I(V_0 + \delta V) = I_0 + \sum_{n=1} I_n \delta V^n / n!$ , where  $I_n = d^n I(V_0) / dV^n$  is the  $n$ th derivative of the  $I-V$  curve around the dc bias,  $V_0$ , across the interface. The nonlinear element acts as a current source at  $n$ th ( $n \geq 2$ ) harmonics of the signal

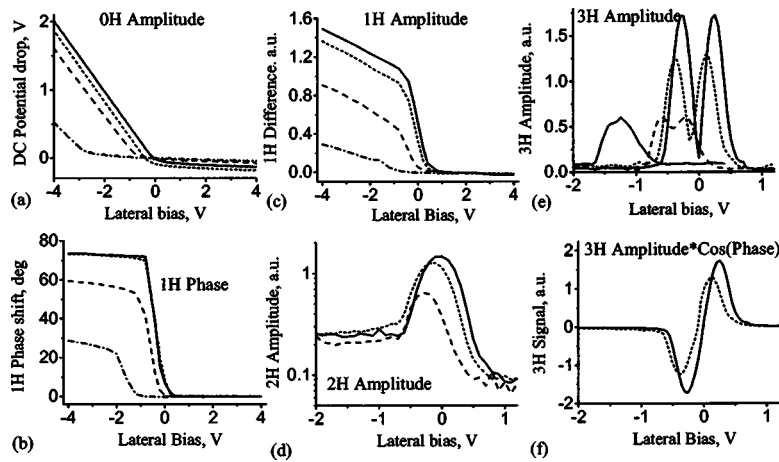


FIG. 3. (a) The dc potential drop across the interface as a function of lateral bias. (b) Phase and (c) amplitude change of the first harmonic signal across the interface. (d) The second harmonic signal on the biased side of the interface. (e) Amplitude and (f)  $x$  component,  $A_{3\omega}\cos(\varphi_{3\omega})$  of the third-harmonic signal. Shown are curves for circuit termination resistances of 1 k $\Omega$  (solid), 3 k $\Omega$  (dot), 10 k $\Omega$  (dash), and 30 k $\Omega$  (dash-dot).

in parallel with nonlinear interface resistance and grounded through circuit termination resistances [Fig. 1(d)]. For a symmetric circuit, the amplitudes of the intrinsic second and third harmonic of the signal [first terms in Eqs. (3a)–(3c)] are equal on both sides of the interface, whereas, for current conservation, the phase changes by 180°. The numerical value of the amplitude is directly related to the second and third derivatives of the  $I$ – $V$  curve as

$$V_{2\omega} = \frac{I_2 R}{(1 + 2I_1 R)^3} V_{ac}^2, \quad (4a)$$

$$V_{3\omega} = \left[ \frac{I_3 R}{3(1 + 2I_1 R)^4} - \frac{2I_2^2 R^2}{(1 + 2I_1 R)^5} \right] V_{ac}^3. \quad (4b)$$

For small circuit termination resistances,  $I_1 R \ll 1$ , Eqs. (4a) and (4b) indicate that the measured second and third harmonic signals provide direct information on the second,  $I_2(V_0)$ , and third,  $I_3(V_0)$ , derivatives of the  $I$ – $V$  curve as a function of dc bias across the interface. Thus, nonlinear transport properties of electroactive interfaces can be evaluated from the measurements of nonlinear voltage harmonics as a function of the lateral dc bias.

This nonlinear transport spectroscopy is illustrated in Fig. 3. The dc potential drop across the interface can be determined as a function of lateral bias [Fig. 3(a)]. Amplitude and phase of the first harmonic signal across the interface are directly related to linear interface resistance and capacitance as illustrated in Figs. 3(b) and 3(c). The dc bias dependence of the second harmonic signal is shown in Fig. 3(d). Note that from Eq. (3b) the latter has contributions from both  $V_{1\omega}$  and  $V_{2\omega}$ . From comparison of Figs. 3(c) and 3(d), it is clear that the peak of  $V_{2\omega}$  for  $V_{lat} \sim 0$  is due to the intrinsic nonlinearity of the interface rather than due to the second harmonic generation in the tip–surface junction, whereas for large negative biases the tip–surface junction contribution [the second term in Eq. (3b)] dominates. Depending on the dc bias, the intrinsic term can be an order of magnitude larger than the tip–surface junction term. For  $R = 1, 3,$  and  $10$  k $\Omega$  the magnitude of  $V_{2\omega}$  depends on  $R$  only weakly, in agreement with the above-mentioned assumption ( $I_1 R \ll 1$ ). The lateral bias dependence of  $V_{3\omega}$  is illustrated in Figs. 3(e) and 3(f). The observed behavior stems from the

fact that  $V_{3\omega}$  is proportional to the derivative of  $V_{2\omega}$  for small  $R$ , while for higher resistances, the full Eq. (4b) must be used.

In conclusion, we demonstrate that nonlinear transport properties of electroactive interfaces can be experimentally accessed using nonlinear SIM. Both intrinsic frequency mixing in the device and electrostatic frequency mixing in the tip–surface junction contribute to the measured signal. The third harmonic signal is independent of tip properties and is a signature of nonlinear behavior of the circuit. For small termination resistance, the second and third harmonics of the voltage signal are related to the corresponding derivatives of the interface  $I$ – $V$  curve. The signal-to-noise ratio can be improved by using first and second resonance frequencies of the cantilever for the electrostatic and topographic detection, respectively. Although nonlinear properties are generally too complex in macroscopic techniques,<sup>11</sup> nonlinear SIM allows spatially resolved imaging of nonlinear transport properties and provides an extended approach for quantitative nanoscale characterization of nonlinear transport phenomena.

Research performed as a Eugene P. Wigner Fellow and staff member at ORNL (S.V.K.). Support from ORNL Laboratory Research and Development funding is acknowledged (V.M., A.P.B., and S.V.K.). V.M. acknowledges support from the Mathematical, Information and Computational Sciences Division, Office of Advanced Scientific Computing Research of the U.S. Department of Energy. Oak Ridge National Laboratory is managed by UT-Battelle, LLC, for the U.S. Department of Energy under Contract No. DE-ACO5-000R22725.

<sup>1</sup>S. M. Sze, *Physics of Semiconductor Devices* (Wiley, New York, 1981).

<sup>2</sup>L. L. Hench and J. K. West, *Principles of Electronic Ceramics* (Wiley, New York, 1990).

<sup>3</sup>A. Hagfeldt and M. Graetzel, *Acc. Chem. Res.* **33**, 269 (2000).

<sup>4</sup>M. Ziese, *Rep. Prog. Phys.* **65**, 143 (2002).

<sup>5</sup>S. J. Tans and C. Dekker, *Nature (London)* **404**, 834 (2000).

<sup>6</sup>A. Chavez-Pirson, O. Vatel, M. Tanimoto, H. Ando, H. Iwamura, and H. Kanbe, *Appl. Phys. Lett.* **67**, 3069 (1995).

<sup>7</sup>S. V. Kalinin and D. A. Bonnell, *J. Appl. Phys.* **91**, 832 (2002).

<sup>8</sup>B. D. Huey and D. A. Bonnell, *Appl. Phys. Lett.* **76**, 1012 (2000).

<sup>9</sup>S. V. Kalinin and D. A. Bonnell (unpublished).

<sup>10</sup>S. V. Kalinin and D. A. Bonnell, *Appl. Phys. Lett.* **78**, 1306 (2001).

<sup>11</sup>*Impedance Microscopy: Emphasizing Solid Materials and Systems*, edited by J. R. Macdonald (Wiley, New York, 1987).